ChemComm

COMMUNICATION

View Article Online
View Journal | View Issue

Cite this: *Chem. Commun.*, 2021, 57, 1214

Received 15th October 2020,
Accepted 14th December 2020

DOI: 10.1039/d0cc06717b

rsc.li/chemcomm

A twin-axial pseudorotaxane for phosphorescence cell imaging†

Xin-Kun Ma,[a] Ying-Ming Zhang,[a] Qilin Yu,[b] Haoyang Zhang,[a] Zhiyuan Zhang[a] and Yu Liu *[a]

A twin-axial pseudorotaxane is constructed using a phenylpyridine salt with diethanolamine (DA-PY) and cucurbit[8]uril (CB[8]), and it not only displays phosphorescence in aqueous solution but it can also be used for targeted cell-imaging.

Pure organic room-temperature phosphorescence (RTP) has received great attention because of its potential applications in biological imaging,[1–4] light-emitting devices,[5] information storage and encryption,[6,7] and other fields. Many well-designed pure organic phosphorescent molecules have been developed, and the key design principle for RTP molecules is regarded as overcoming the inefficient spin–orbit coupling and avoiding quenching of the triplet excited state.[8] For example, the introduction of a heavy atom can trigger significant intersystem crossing (ISC),[9] and halogen bonding promotes ISC by reducing the molecular motion and enhancing the heavy-atom effect.[10] However, it is still difficult to achieve phosphorescence in water, especially with compounds that completely dissolve in solution, because the phosphorescence is easily quenched by oxygen and water. Several methods have been reported to achieve RTP in water, such as polymerization,[11–13] solid dispersion,[14] and host–guest interaction.[12,13,15–17] Wu and co-workers used a nanoprecipitation method to prepare nanoparticles that showed RTP in water and effective imaging towards cells.[14] Tian and co-workers have made great contributions to phosphorescence using supramolecular assembly. For example, strong RTP luminescence in the amorphous solid state was achieved by modifying β-CDs, and the hydrogen bonding between the cyclodextrin derivatives could suppress the non-radiative relaxation and enhance phosphorescence emission.[15,16] Kim and co-workers reported a strategy to enhance phosphorescence *via* intermolecular interactions (halogen and hydrogen bonding).[18,19] Additionally, we also reported an efficient way to improve quantum yield and lifetime in the solid state and its application in anti-counterfeiting.[20,21] However, phosphorescence in aqueous solution still requires more attention, especially in biological sensing and imaging, because in aqueous media, electrons of the organic RTP luminophores in the triplet excited state can be easily quenched by molecular motion and oxygen. On the other hand, suitable size, good solubility in water, and biocompatibility should also be taken into consideration.[8] Herein, we report a water-soluble twin-axial pseudorotaxane based on host–guest recognition between a cucurbit[8]uril and a phenylpyridine derivative (DA-PY). This pseudorotaxane can emit effective phosphorescence in aqueous solution. The binding mode of the pseudorotaxane and its luminescence properties were investigated by means of isothermal titration calorimetry (ITC), mass spectrometry, NMR, ultraviolet-visible, fluorescence, and phosphorescence measurements, along with structural optimization calculations. The results revealed the molecular structure of the "two-end blocked" pseudorotaxane. Phosphorescence might result not only from the introduction of a heavy atom, which enhances the ISC rate, but also from the "pseudorotaxane" structure, which strengthens the halogen bonding and reduces non-radiative transitions. Additionally, the pseudorotaxane was successfully used for cell imaging targeted at mitochondria.

Assemblies consisting of phenylpyridine derivatives and cucurbit[6]uril (CB[6]) can display efficient phosphorescence in the solid state,[20,21] but they would not be suitable in water because CB[6] has poor solubility in water, even when binding a guest. Moreover, oxygen and water would affect the phosphorescence more obviously when the complexes are dissolved in solution. Thus, we speculated that assemblies based on CB[8], which has a similar structure to CB[6] and better solubility, could achieve effective phosphorescence in water. To verify this hypothesis, a phenylpyridine derivative (DA-PY) was designed and synthesized (Scheme 1).

DA-PY exhibits a strong absorption peak at 310 nm and a blue fluorescence emission peak at 384 nm in water (Table S1,

[a] *College of Chemistry, State Key Laboratory of Elemento-Organic Chemistry, Nankai University, Tianjin 300071, P. R. China. E-mail: yuliu@nankai.edu.cn*
[b] *Key Laboratory of Molecular Microbiology and Technology, College of Life Sciences, Nankai University, Tianjin, P. R. China*

† Electronic supplementary information (ESI) available. See DOI: 10.1039/d0cc06717b

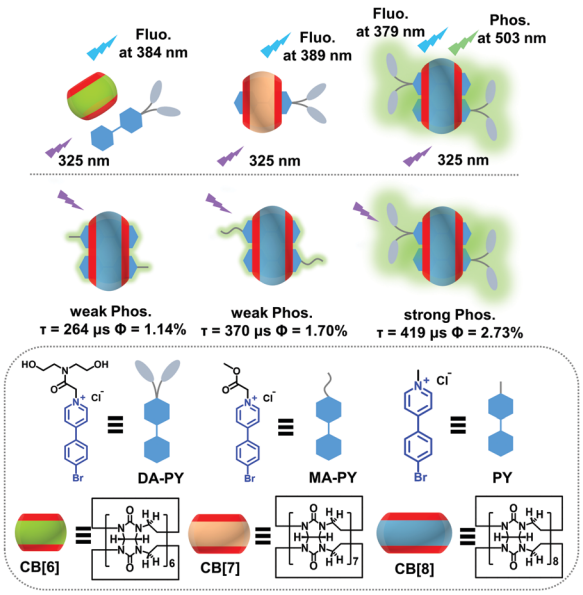

Scheme 1 A schematic illustration of the phosphorescent supramolecular assembly.

ESI†). Surprisingly, a new peak (503 nm) appeared and became stronger as CB[8] was added to the solution of DA-PY (Fig. 1a and Fig. S1d, ESI†). The resulting phosphorescence lifetime was 419 μs (Fig. 1b), and the phosphorescence quantum yield was 2.73%. The microsecond-order lifetime provides strong evidence of phosphorescence. Furthermore, the phosphorescence properties of DA-PY/CB[8] in the solid state were also characterized (Fig. S22, ESI†); a longer lifetime was observed, which is consistent with our previous work. Further evidence confirming that the emission at 503 nm was phosphorescence was obtained. To weaken the phosphorescence quenching effect of dissolved oxygen, the DA-PY/CB[8] solution was vacuum-degassed. The intensity of the peak at 503 nm increased greatly (Fig. S1f, ESI†), and it showed a longer lifetime (944 μs) (Fig. S23, ESI†). The peak at 503 nm was more obviously enhanced than that at 390 nm when the temperature of the solution was decreased from 343 K to 273 K (Fig. S1g, ESI†), and the lifetime at 510 nm accordingly changed from 225 μs to 760 μs (Fig. S1h, ESI†). In addition, low-temperature spectroscopy of a solid powder of the guest was conducted. DA-PY showed obvious phosphorescence at 77 K, which is consistent with the previous report and further suggested that the phosphorescence originates from the guest.[20]

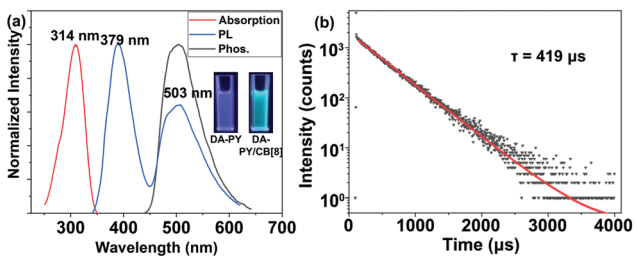

Fig. 1 (a) The photophysical properties of DA-PY/CB[8]. (a) Excitation (red), fluorescence (blue) and phosphorescence (black) spectra of DA-PY/CB[8] in solution (λ_{ex} = 325 nm, [CB[8]] = 30 μM and [DA-PY] = 60 μM); insets: Photographs of the luminescence of DA-PY (1.00 mM) and DA-PY/CB[8] (1.0 mM) in solution at 298 K under UV (365 nm) light. (b) Time-resolved photoluminescence decay and fitting curves of DA-PY/CB[8] solution ([CB[8]] = 30 μM and [DA-PY] = 60 μM) at 510 nm at room temperature.

It is well-known that the introduction of heavy atoms can facilitate ISC and improve the phosphorescence quantum yield, as the heavy-atom effect can promote the probability of S_1–T_n intersystem crossing and cause spin–orbit coupling (SOC). However, phosphorescence could not be detected in solutions of DA-PY, DA-PY/CB[6], DA-PY/CB[7] and CB[6, 7, 8] (Fig. S1 and S27, ESI†). Thus, factors other than the introduction of heavy atoms are responsible for the enhanced phosphorescence: (1) the rigidified cavity structure of cucurbituril can provide a good hydrophobic cavity and protect the chromophore from water and oxygen attack; (2) the DA-PY/CB[8] assembly is more stable and tighter than DA-PY/CB[6] and DA-PY/CB[7] in solution; (3) hydrogen bonding between CB[8] and DA-PY made the pseudorotaxane structure tighter; (4) the inclusion form of the assembly promotes halogen bonding by shortening the distance between the bromine and carbonyl groups.

In the UV-Vis spectra, the maximum absorption was red-shifted upon the addition of CB[7] or CB[8] (Fig. S11, ESI†), implying that DA-PY formed assemblies with CB[7] and CB[8]. In the fluorescence spectra of DA-PY, after binding with CB[6], the fluorescence intensity was slightly enhanced (Fig. S1b, ESI†), suggesting that the DA-PY was included in CB[6] in a small amount. With the addition of CB[7], the fluorescence of the solution exhibited a significant improvement (Fig. S1c, ESI†) because of the good water solubility and reduced non-radiative transition. However, when CB[8] was continuously added to a solution of DA-PY, the fluorescence peak decreased (Fig. S1d, ESI†) and the phosphorescence peak increased; additionally, the luminescence color of the solution changed from blue to green (Fig. 1a, inset). This implies a transition from fluorescence to phosphorescence because the formation of the DA-PY/CB[8] assembly enhanced and activated the phosphorescence.

In order to prove that the assembly structure of DA-PY/CB[8] with the "head-to-tail" and "one host with two guests" modes was the main source of the phosphorescence in the aqueous solution (Scheme 1), the Job's plot method was adopted to validate the binding stoichiometry between DA-PY and CB[8]. An inflection point was observed at a molar ratio of 0.66, indicating a 2 : 1 binding stoichiometry (Fig. S2b, ESI†). In addition, the CB[7] *vs.* DA-PY curve exhibited an inflection point at 0.5, which implies a 1 : 1 binding stoichiometry between CB[7] and DA-PY (Fig. S2a, ESI†). Mass spectrometry also demonstrated the formation of the DA-PY/CB[8] complex (Fig. S4, ESI†). The intense $[M - 2Cl + H]^{2+}$ peak (m/z 1045.5) fit well with the calculated value (1045.7). ^{1}H NMR spectra in which different numbers of equivalents of CB[8] were added to the solution of DA-PY were recorded, and the original peak disappeared completely when [CB[8]]/[DA-PY] was equal to 0.5; this result was in good agreement with the Job's plot results (Fig. S6, ESI†). In addition to the poor solubility of CB[6],

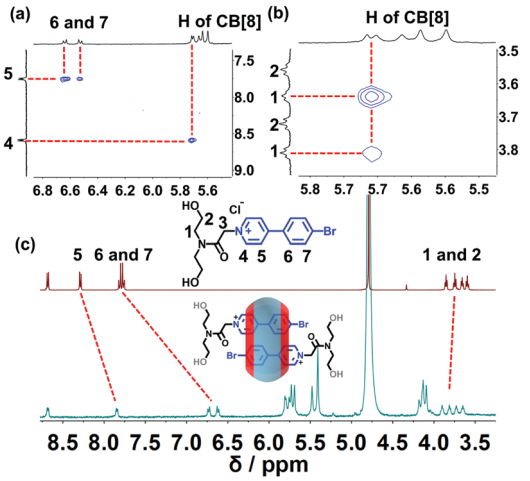

Fig. 2 (a and b) 2D ROESY spectra (400 MHz, D_2O, 298 K) of DA-PY/CB[8] ([DA-PY] = 5.0 mM, [CB[8]] = 2.5 mM); (c) ^{1}H NMR (400 MHz, D_2O, 298 K) spectra of solutions of DA-PY (red) and DA-PY/CB[8] (green); [DA-PY] = [DA-PY/CB[8]] = 10.0 μM.

the binding between CB[6] and DA-PY was weak, and the aromatic protons shifted to lower field after the addition of excess CB[6] under long-time ultrasonic dissolution, suggesting that DA-PY might be expelled from the CB[6] cavity (Fig. S9, ESI†). Furthermore, 2D ROESY provided more powerful evidence of the formation of the inclusion complex (Fig. 2 and Fig. S10, ESI†). Strong signals were observed between the H_5 protons of pyridine and the $H_{6,7}$ protons of the phenyl group, implying that DA-PY was present in the CB[8] cavity in a "head-to-tail" manner. The "head-to-tail" arrangement not only decreases the distance between the carbonyl and halogen groups of the two guest molecules, but also facilitates the interaction between the carbonyl of cucurbituril and halogen. More evidence was provided by the binding constant (K_s). Using ITC and UV titration, the K_s values for the DA-PY/CB[8] and DA-PY/CB[7] complexes were estimated to be 8.60×10^{11} M^{-2} and 2.50×10^{6} M^{-1}, respectively (Fig. S11 and S24, ESI†). The larger binding constant suggested a more stable and tighter structure, which could effectively reduce the non-radiative transitions caused by molecular motion. In summary, the poor solubility of the DA-PY/CB[6] complex and the looser structure of the DA-PY/CB[7] complex would not promote the generation of phosphorescence.

Moreover, the $H_{1,2}$ protons shifted downfield in the ^{1}H NMR spectrum, and the H_1 protons of DA-PY exhibited correlation peaks with the H_a protons of CB[8] (Fig. 2b) in the 2D ROESY spectrum. This phenomenon implied that hydrogen bonds might exist between the hydroxyl and carbonyl groups, and that the stoppers of the pseudorotaxane, *i.e.*, the hydroxyl groups of diethanolamine, might contribute to the formation of a more stable assembly. Subsequently, MA-PY and PY without modification with diethanolamine were designed (Scheme S1, ESI†). MA-PY, PY and DA-PY had similar optical properties due to having the same luminophore (Table S1, ESI†). In addition, the molecular binding behaviors of MA-PY were similar to those of DA-PY upon complexation with CB[6] and CB[7]. The corresponding characterization results are given in the ESI.† Notably, DA-PY/CB[8] had a higher phosphorescence quantum yield and longer lifetime than MA-PY/CB[8] (Φ_{Phos} = 1.70%, τ_{phos} = 370 μs) and PY (Φ_{Phos} = 1.14%, τ_{phos} = 264 μs) (Table S1, ESI†). PY did not form intermolecular halogen bonds, resulting in a small k_{isc} (Table S1, ESI†). Not only did the halogen bond play an important role in the enhancement of the phosphorescence, but the hydrogen bonding between the host and the guests also had a positive effect. The reasons for the stronger phosphorescence were provided by the binding constant and density functional theory (DFT) calculations. The K_s value of MA-PY/CB[8] was calculated to be 4.58×10^{11} M^{-2}, which was smaller than that of DA-PY/CB[8] (8.60×10^{11} M^{-2}) (Fig. S24, ESI†). This result was mainly due to the hydrogen-bonding interconnection between the host and guests, which made the resulting ternary complexes more stable.

In the DFT and TD-DFT results, the hydrogen bonds of the pseudorotaxane shortened the distance between the bromine and carbonyl groups. The distance between $Br_{DA\text{-}PY}\cdots O{=}C_{DA\text{-}PY}$ (bromine and the carbonyl of the other DA-PY) is 3.43 Å, and that of $Br_{DA\text{-}PY}\cdots O{=}C_{CB[8]}$ (bromine and the carbonyl of CB[8]) is 3.30 Å, which is shorter than $Br_{MA\text{-}PY}\cdots O{=}C_{MA\text{-}PY}$ (3.50 Å) and $Br_{MA\text{-}PY}\cdots O{=}C_{CB[8]}$ (3.86 Å) (Fig. 3a and b). According to the frontier molecular orbital (FMO) analysis, DA-PY had more LUMO overlap and a smaller energy gap (5.98 eV) between the HOMO and LUMO than MA-PY (6.25 eV) due to the extensive hydrogen-bonding interactions in the structure of pseudorotaxane. Stronger halogen bonding and a reduced distance between the bromine and carbonyl can promote ISC by reducing ΔE_{ST} (the energy gap between S_1 and T_n).[10] DA-PY/CB[8] had much a smaller ΔE_{ST} (0.055 eV) than DA-PY (0.254 eV) and MA-PY/CB[8] (0.251 eV) (Fig. 3c–e), which suggested that the stronger halogen bond promoted ISC and SOC. The k_{isc} value was further estimated according to perturbation theory and previous work:[22]

$$k_{isc} \propto \left|\langle S|\hat{H}_{SOC}|T\rangle\right|^2 \exp\left(-\Delta E_{ST}{}^2\right)$$

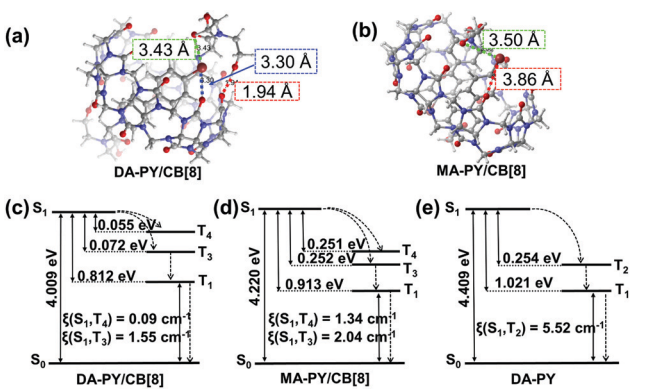

Fig. 3 Theoretical calculations of the phosphorescence emission mechanism. (a and b) The optimized structures and intermolecular interactions of DA-PY/CB[8] and MA-PY/CB[8]. The dotted lines in the figure are the distances between Br···O=C and OH···O=C. (c–e) Energy level diagrams and SOC coefficients for DA-PY/CB[8], MA-PY/CB[8] and DA-PY in the aqueous state.

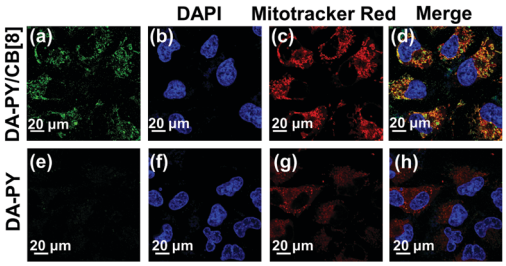

Fig. 4 Confocal fluorescence images of human lung adenocarcinoma A549 cells co-stained with DA-PY/CB[8] and DA-PY ([DA-PY] = 0.05 mM, [CB[8]] = 0.01 mM), DAPI (nuclear probe, 0.005 mM), and Mitotracker Red (mitochondria probe, 0.005 mM) for 30 min: (a) DA-PY/CB[8] (ex. 315 nm, em. 520 nm); (b) DAPI (ex. 358 nm, em. 461 nm); (c) mitotracker Red (ex. 579 nm, em. 599 nm); (d) a merged image of (a–c); (e–h) are similar to (a–d) but using DA-PY alone.

when the ξ_{ST} (SOC coefficients) were similar, the k_{isc} of DA-PY/CB[8] was larger than that of MA-PY/CB[8], but with a much smaller ΔE value. The larger k_{isc} could facilitate the electron transfer from the S_1 excited state to the T_n excited state through the ISC pathway. Taken together, the presence of hydrogen bonds could make the pseudorotaxane more stable and enhance intermolecular interactions, and more importantly, these interactions would be beneficial to phosphorescence emission.

Considering that phosphorescent imaging has the obvious advantages of lower background interference and a longer lifetime than fluorescence imaging, we expected that the DA-PY/CB[8] pseudorotaxane might display good performance in cellular imaging. Confocal laser scanning microscopy of A549 cells incubated with DA-PY/CB[8] and the DA-PY monomer suggested that the DA-PY/CB[8] assemblies could be easily internalized into the cell and displayed an effective green phosphorescence, which showed a good colocalization with the mitochondria marker Mitotracker Red (Fig. 4d).

These results indicated that the DA-PY/CB[8] assembly is an effective phosphorescent imaging probe for mitochondria in living cells. We speculated that this specific organelle targeting might be attributed to the efficient positive charges of DA-PY and the hydrophobic construction of cucurbituril. Moreover, it is known that high cytotoxicity imaging agents limit the application of cellular probes. Therefore, we investigated the cell cytotoxicity of the DA-PY/CB[8] assembly using MTT assays. When the concentration was below 0.01 mM ([CB[8]] = 0.01 mM, [DA-PY] = 0.05 mM, respectively), the complex showed almost no toxicity to A549 cells (cancer cell line) or NIH3T3 cells (normal cell line) (see the ESI†). Additionally, DA-PY/CB[8] displayed lower toxicity than DA-PY even when the concentration was increased to 0.2 mM. In summary, the formation of the pseudorotaxane assembly not only promotes the generation of phosphorescence, but also reduces the biological toxicity and achieves good targeted imaging.

We have constructed a twin-axial pseudorotaxane with good water solubility based on host–guest interactions between DA-PY and CB[8], and it displayed effective pure organic RTP with a long lifetime ($\tau_{DA\text{-}PY/CB[8]}$ = 419 μs). The phosphorescence relies on a pseudorotaxane structure featuring a "head-to-tail" and "one host with two guests" binding mode, and the cooperative hydrogen-bonding interaction between the hydroxyl of DA-PY and carbonyl of CB[8] could further enhance the phosphorescence. Additionally, the obtained 1 : 2 complexes were successfully used for the targeted mitochondria cell imaging of living cells with low bio-toxicity. These results might help us to design more advanced phosphorescent assemblies for cell imaging and diagnostics.

This work was financially supported by the National Natural Science Foundation of China (grant no. 21672113, 21772099, 21861132001 and 21971127).

Conflicts of interest

There are no conflicts to declare.

Notes and references

1 S. M. A. Fateminia, Z. Mao, S. Xu, Z. Yang, Z. Chi and B. Liu, *Angew. Chem., Int. Ed.*, 2017, **56**, 12160–12164.
2 A. Nicol, R. T. K. Kwok, C. Chen, W. Zhao, M. Chen, J. Qu and B. Z. Tang, *J. Am. Chem. Soc.*, 2017, **139**, 14792–14799.
3 J. Yang, X. Zhen, B. Wang, X. Gao, Z. Ren, J. Wang, Y. Xie, J. Li, Q. Peng, K. Pu and Z. Li, *Nat. Commun.*, 2018, **9**, 840.
4 J. Wang, Z. Huang, X. Ma and H. Tian, *Angew. Chem., Int. Ed.*, 2020, **59**, 9928–9933.
5 X. Yang, G. Zhou and W.-Y. Wong, *Chem. Soc. Rev.*, 2015, **44**, 8484–8575.
6 Z. An, C. Zheng, Y. Tao, R. Chen, H. Shi, T. Chen, Z. Wang, H. Li, R. Deng, X. Liu and W. Huang, *Nat. Mater.*, 2015, **14**, 685–690.
7 Y. Su, S. Z. F. Phua, Y. Li, X. Zhou, D. Jana, G. Liu, W. Q. Lim, W. K. Ong, C. Yang and Y. Zhao, *Sci. Adv.*, 2018, **4**, eaas9732.
8 Kenry, C. Chen and B. Liu, *Nat. Commun.*, 2019, **10**, 2111.
9 C. A. DeRosa, S. A. Seaman, A. S. Mathew, C. M. Gorick, Z. Fan, J. N. Demas, S. M. Peirce and C. L. Fraser, *ACS Sens.*, 2016, **1**, 1366–1373.
10 O. Bolton, K. Lee, H.-J. Kim, K. Y. Lin and J. Kim, *Nat. Chem.*, 2011, **3**, 205–210.
11 X. Ma, C. Xu, J. Wang and H. Tian, *Angew. Chem., Int. Ed.*, 2018, **57**, 10854–10858.
12 H. Chen, X. Ma, S. Wu and H. Tian, *Angew. Chem., Int. Ed.*, 2014, **53**, 14149–14152.
13 J.-J. Li, H.-Y. Zhang, Y. Zhang, W.-L. Zhou and Y. Liu, *Adv. Opt. Mater.*, 2019, **7**, 1900589.
14 X.-F. Wang, H. Xiao, P.-Z. Chen, Q.-Z. Yang, B. Chen, C.-H. Tung, Y.-Z. Chen and L.-Z. Wu, *J. Am. Chem. Soc.*, 2019, **141**, 5045–5050.
15 Y. Gong, H. Chen, X. Ma and H. Tian, *ChemPhysChem*, 2016, **17**, 1934–1938.
16 L. Xu, L. Zou, H. Chen and X. Ma, *Dyes Pigm.*, 2017, **142**, 300–305.
17 M. González-Béjar, P. Montes-Navajas, H. García and J. C. Scaiano, *Langmuir*, 2009, **25**, 10490–10494.
18 M. S. Kwon, D. Lee, S. Seo, J. Jung and J. Kim, *Angew. Chem., Int. Ed.*, 2014, **53**, 11177–11181.
19 D. Lee, O. Bolton, B. C. Kim, J. H. Youk, S. Takayama and J. Kim, *J. Am. Chem. Soc.*, 2013, **135**, 6325–6329.
20 Z.-Y. Zhang, Y. Chen and Y. Liu, *Angew. Chem., Int. Ed.*, 2019, **58**, 6028–6032.
21 Z.-Y. Zhang and Y. Liu, *Chem. Sci.*, 2019, **10**, 7773–7778.
22 H. Ma, Q. Peng, Z. An, W. Huang and Z. Shuai, *J. Am. Chem. Soc.*, 2019, **141**, 1010–1015.